Analysis of wake effects on global responses for a floating two-turbine case

IOP Conf. Series: Journal of Physics: Conf. Series **1356** (2019) 012004 doi:10.1088/1742-6596/1356/1/012004

Analysis of wake effects on global responses for a floating two-turbine case

A Wise[1] and E E Bachynski[1]

[1]Department of Marine Technology, Norwegian University of Science and Technology, Otto Nielsens veg 10, 7052 Trondheim, Norway

E-mail: adamsw@stud.ntnu.no

Abstract.

While most existing modeling and analysis of floating wind turbines (FWTs) considers isolated systems, interactions among multiple FWTs arranged in an array have received little attention. In this study, two 10 MW semi-submersible FWTs, separated by 8 rotor diameters (D) in the wind direction, are simulated with an ambient wind speed of 10 m/s and in moderate wave conditions using FAST.Farm to investigate the effects of wakes on global responses. Synthetic inflow is generated using three methods: the Kaimal turbulence model, 1) without and 2) with spatial coherence in the lateral and vertical velocity components, and 3) the Mann turbulence model (where spatial coherence in all three dimensions is inherent to the model). The first method results in negligible wake meandering, a relatively uniform wake deficit, while the second and third methods result in meandering of the upstream turbine's lateral wake center at the downstream turbine's rotor plane of up to approximately $1D$ and $1.5D$, respectively. The slow meandering behavior of the upstream turbine's wake resulted in increased low-frequency platform motions for the downstream turbine. Yaw motions were especially susceptible to wake meandering as the standard deviation of the downstream turbine's yaw motion increased by 28.0 % for the second method and 11.3 % for the third method. Increased low-frequency response in structural loading was also observed. Wake effects led to between 2 % and 30 % greater fatigue damage at the top of the tower for all three methods and at the base of the tower for the second method. However, other results were found to be sensitive to the blade-passing frequency.

1. Introduction

Floating wind turbines (FWTs) represent the next generation of offshore wind turbines. Since bottom-fixed offshore wind turbines are only economically viable in shallow to intermediate water depths, FWTs will be used to harness the wind resource in deep water. As a result, the modeling of FWT concepts, such as semi-submersibles, spars, and tension-leg platforms, has progressed significantly in recent years. However, most state-of-the-art analysis has been conducted for single systems without consideration of the wake interaction from nearby FWTs. The first floating wind farm, Hywind Scotland, began producing electricity in October 2017 [1] and as more floating wind farms are being developed, understanding the effects of wakes on the motions and loading of FWTs may have a significant impact on farm layout and both wind turbine and farm control systems.

Wind turbine operation induces a downstream decrease in wind speed and increase in turbulence intensity. Wind turbines that are subjected to the wake of upstream wind turbines

produce less power and often experience greater structural loading. These wake effects have long been known empirically [2, 3], but only within the past decade have researchers found success numerically modeling the dynamic behavior of wakes [4–6]. A significant amount of research has been conducted on wake effects for onshore and bottom-fixed offshore systems [7–9], but little has been done with regards to FWTs. Compared to onshore and bottom-fixed systems, FWTs will have different dynamic responses. Additionally, FWTs have long natural periods in certain degrees of freedom, which may be excited by the low-frequency meandering behavior of the wake across the rotor when using a dynamic wake meandering (DWM) model.

FAST.Farm is a new wind farm multiphysics modeling tool that has been developed by the National Renewable Energy Laboratory (NREL) [10]. Instances of OpenFAST (the latest version of FAST [11]) within FAST.Farm model the nonlinear, dynamic behavior of distinct turbines. Especially important to FWTs, FAST.Farm includes wind turbine motion when updating the wake deficit and center line. While FAST.Farm was originally developed to compute the ambient wind farm-wide using a precursor large-eddy simulation, recent updates allow the inflow to be generated more easily using a synthetic turbulent wind model e.g. TurbSim [12] or the Mann model in the IEC turbulence simulator [13].

To provide insight into floating wind farm siting and control development, the current work models two DTU 10 MW wind turbines each supported by identical semi-submersible platforms in FAST.Farm. The upstream turbine operates under normal conditions while the second turbine, located 8 rotor diameters (D) downstream, operates in waked conditions. Section 2 describes the OpenFAST model and the FAST.Farm model of the two-turbine case. Three different methods were used to generate synthetic turbulent inflow, resulting in different wake meandering patterns. Representative operational conditions were chosen in order to directly investigate the effects of wakes on motions and on short-term fatigue predictions for the tower and mooring lines. Simulation results are presented and discussed in Section 3, followed by conclusions and future work in Section 4.

2. Methods

2.1. OpenFAST Model

The FWT model used in OpenFAST is the DTU 10 MW reference turbine supported by the CSC semi-submersible platform [14] (together referred to as the CSC 10 MW in this paper), which is based on the original 5 MW platform designed at the Norwegian University of Science and Technology [15]. As prescribed in the design for this FWT, the original, onshore tower of the DTU 10 MW [16] is used. The rotor diameter is still $D = 178.3$ m; however, the structural design of the blades is slightly different than that of the original design and was developed by the Technical University of Munich's Wind Energy Institute [17, 18].

A visualization of the CSC 10 MW in OpenFAST (with lines representing the prebent blades) is depicted in Figure 1. The wind turbine sits on a center column, which is connected by pontoons to the three offset columns, each of which has an attached catenary mooring line. The CSC 10 MW is a braceless type of semi-submersible platform which uses less steel and avoids complex fabrication work required by other semi-submersible designs. Parameters relevant to the design of the CSC hull are given in Table 1.

The CSC 10 MW was developed using SINTEF Ocean's SIMA software. The model has been adapted into the FAST-framework and the important natural periods obtained through decay tests in the two modeling approaches are described in Table 3. Some small differences in the natural periods are observed, but these are not expected to result in large changes in the responses. The first fore-aft tower bending mode is coupled with the pitch motion of the floating platform, and two periods are observed in the OpenFAST decay test results due to phasing with the blades: one at 2.24 s (0.44 Hz) and another at 2.54 s (0.39 Hz). These frequencies are within the blade-passing frequency (3P) range, which is a common design issue for large FWTs. For

example, the LIFES50+ OO-Star Wind Floater Semi 10 MW FWT [19] tower eigenfrequencies were increased to above the 3P range, but this resulted in roughly doubling the tower's mass. In this study, we have made no modifications to the tower structural properties of the CSC 10 MW. However, other studies have adjusted the tower in order to avoid 3P excitation at the tower natural frequency [20].

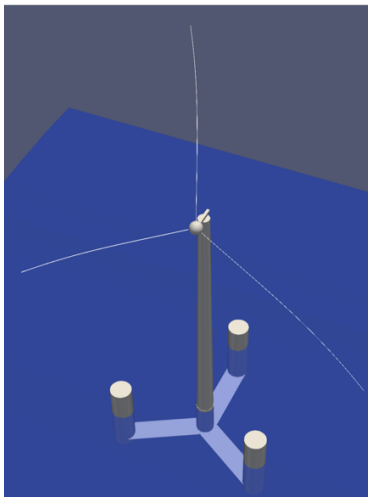

Figure 1: Computational model of the CSC 10 MW visualized in OpenFAST with lines representing the prebent blades.

Table 1: CSC hull dimensions and parameters.

Water Depth	200 m
Displacement	13700 m^3
Center column diameter	8.3 m
Side column diameter	10.0 m
Draft	20.0 m
Center-center distance	45.0 m
Pontoon height	7.0 m
Pontoon width	10.0 m

Table 2: CSC 10 MW mooring dimensions and parameters.

Number of lines	3
Unstretched line length	880 m
Mass/length in air	466 kg/m
Equivalent diameter	153 mm
Pretension at fairlead	2800 kN
Anchor radius	879.6 m

Table 3: CSC 10 MW natural periods and frequencies in OpenFAST and SIMA.

Degree of Freedom	SIMA (s)	OpenFAST (s)	SIMA (Hz)	OpenFAST (Hz)
Surge	88.3	85.1	0.011	0.012
Heave	20.3	20.0	0.049	0.050
Pitch	26.3	24.8	0.038	0.040
Yaw	60.4	58.5	0.016	0.017
Coupled pitch and tower bending	2.40	2.24, 2.54	0.42	0.44, 0.39

The hydrodynamic model of the CSC 10 MW in OpenFAST includes a combination of first order potential flow (from WAMIT) and Morison's equation. First-order waves and linear wave load models are used as it was found that second-order wave loads have only a minor effect on the dynamic response for this platform, especially for the selected environmental conditions (Section 2.2.3) [14]. Each FWT has three individual catenary lines anchored to the sea floor. The mooring lines are modeled using MoorDyn [21] and are described in Table 2.

The blade pitch controller for the CSC 10 MW has been modified from the land-based controller to avoid negative feedback at the platform pitch natural frequency [4]. The controller parameters were tuned and the resulting K_I and K_p are 0.262, 0.0353 s, respectively. No further adjustments to the blade pitch, generator torque, or yaw controllers have been applied in the present work, but may be considered in the future for mitigating the interaction effects.

2.2. FAST.Farm Model

2.2.1. Simulation Setup Each FAST.Farm simulation uses a $X \times Y \times Z = 7.5$ km $\times$ 1 km $\times$ 350 m domain and a simulation time length of 4,000 s (including a 400 s transient). The main flow direction is along X with the upstream turbine, FWT1, located 1 km from the left boundary and the downstream turbine, FWT2, located $8D$ further downstream. A schematic of the FAST.Farm model with the axes normalized by rotor diameter can be found in Figure 2.

Within FAST.Farm, the low-resolution wind domain used for resolving wakes has a spatial resolution of ΔY, $\Delta Z = 10.0$ m, 10.0 m and a time step of 2 s. To accurately compute structural loading, there is high-resolution wind domain around each FWT that has a spatial resolution increased by a factor of two to ΔY, $\Delta Z = 5.0$ m, 5.0 m and the temporal resolution increased to 1/3 s. Additionally, each OpenFAST instance of an FWT has a time step of 0.00625 s. The wake discretization consists of 160 wake planes per rotor, each with a radial finite-difference spatial resolution of 5 m. There are also a number of changeable model parameters in the "Wake Dynamics" subsection of the FAST.Farm input file; however, no modifications have been made to the default model parameters derived from calibration [22].

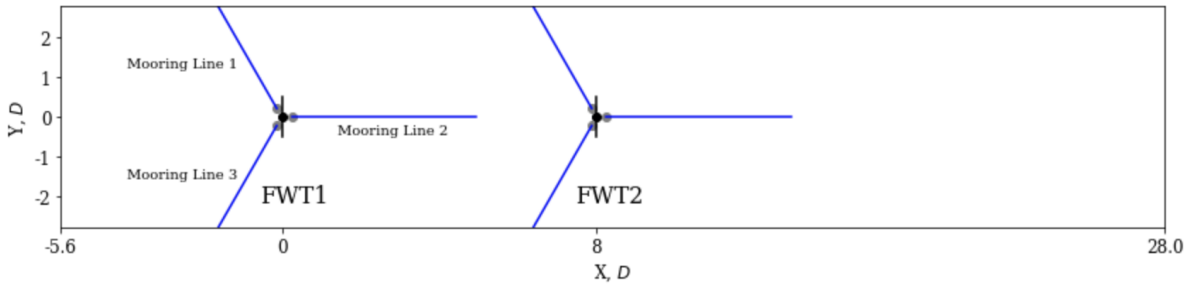

Figure 2: FAST.Farm computational domain normalized by rotor diameter. X has been truncated to 5 km for clarity.

2.2.2. Ambient Wind Generation Offshore wind standards have been adapted from onshore wind standards, where the Kaimal and Mann turbulence models are recommended for the generation of wind fields for simulation of individual turbines [23]. While the two different turbulence models have little impact on the simulated responses for bottom-fixed and onshore wind turbines, previous studies [20, 24, 25] have found that the two models result in different responses for FWTs. The present work is not meant to determine whether one model is more correct than the other, but to compare their effect on the behavior of the wakes and the resulting response of the downstream turbine.

In this study, synthetic turbulent wind data is generated using three different methods. The first two use the Kaimal turbulence model in NREL's TurbSim [12] and the third uses the Mann turbulence model via a turbulence generator (a pre-processor tool to HAWC2) [26]. Both turbulence models make use of the Kaimal spectrum, but their spatial distribution of turbulence differs. The Kaimal turbulence model uses an exponential spatial coherence function:

$$Coh_{i,j_K}(r,f) = \exp\left(-a_K\sqrt{\left(\frac{fr}{\bar{u}_{hub}}\right)^2 + (rb_K)^2}\right) \tag{1}$$

where Coh_{i,j_K} is the spatial coherence between points i and j for the velocity components $K = u$; v; w; r is the distance between points i and j; f is the frequency; a_K is the coherence decrement parameter; and b_K is the coherence offset parameter.

The IEC standard does not provide values of a_K and b_K for the lateral and vertical velocity components. In TurbSim, the default values for a_v, a_w, b_v, and b_w are listed in Table 4 and result in no spatial coherence, and consequently negligible wake meandering [27]. While using the default parameters in TurbSim does not provide realistic wake meandering behavior, the model is included here as the first of the two methods using the Kaimal turbulence model because the minimal wake meandering essentially represents a uniform, axial wake deficit. The results from this method, denoted "Kaimal - Coh u", help to isolate the wake effects specifically related to meandering.

To induce meandering in the second method, we specify values for a_K and b_K (found in Table 4). They are formulated as $a_u = \bar{u}_{hub}$; a_v, $a_w = 0.75\bar{u}_{hub}$; and b_u, b_v, $b_w = 0.0$. The selected values for the second model, which is referred to as "Kaimal - Coh u, v, w", are the default parameters for the Risø Smooth-Terrain turbulence model in TurbSim.

Table 4: Spatial coherence parameters specified in TurbSim.

Model name	a_u (-)	b_u (m^{-1})	a_v (-)	b_v (m^{-1})	a_w (-)	b_w (m^{-1})
Kaimal - Coh u	12.0	3.5273×10^{-4}	∞	0.0	∞	0.0
Kaimal - Coh u, v, w	10.0	0.0	7.5	0.0	7.5	0.0

The third method, referred to as "Mann", uses the Mann turbulence model, which generates turbulence using a spectral tensor, resulting in spatial coherence in all three wind directions. A detailed description of the model can be found in [28]. The model has three parameters that can be used to fit it to a wind spectrum and the turbulence intensity: $\alpha\epsilon^{2/3}$, Γ, and L. To fit the Mann model to the Kaimal spectrum, the values $\alpha\epsilon^{2/3} = 0.10$ $\mathrm{m}^{4/3}\mathrm{s}^{-2}$, $\Gamma = 3.9$ and $L = 33.6$ m are applied, which are in accordance with the IEC standard.

2.2.3. Environmental Conditions The CSC 10 MW was designed for a deep-water (200 m) reference site in the North Sea. Hindcast data of 1-h averaged wind and sea states are used to generate 10-yr wind and wave statistics for the reference site (Site 14 in [29]).

Rotor thrust is a major driver of wake deficits; therefore, a hub-height wind speed (U) of 10 m/s was chosen for the simulations to more easily investigate wake effects. Based on the significant wave height H_s and peak period T_p distributions for a wind speed of 10 ± 1 m/s, $H_s = 2.5$ m and $T_p = 9.5$ s were chosen. Additionally, the most probable shear exponent in these conditions was found to be 0.055.

A wave spectrum in accordance with the IEC 61400-3 standard [30] was used to generate the wave history. Because no information about turbulence can be deduced from the hindcast dataset due its low temporal resolution, the desired hub-height turbulence intensity (TI) used for the simulations was set to 15.72 % as defined by the IEC 61400-1 standard [23] for a wind speed of 10 m/s (Class C site). A summary of the environmental conditions can be found in Table 5.

Table 5: Environmental conditions.

H_s (m)	T_p (s)	U (m/s)	TI (%)	Shear Exponent (-)
2.5	9.5	10	15.72	0.055

2.3. Fatigue Analysis

The IEC standard for offshore wind turbines recommends six simulations of ten minutes in duration or a continuous one hour simulation [30]. Six 1-h simulations (after a 400-s transient)

are used to capture the effects of the long natural periods and the stochastic variation in the results. Additionally, a study of a similar semi-submersible found that six 1-h simulations captured the contribution of a given environmental condition to the lifetime (20-yr) tower fatigue damage within 3 % [31].

Using the time-history of loads at the tower base and tower top, the axial stress σ at a given point on the cross section (r, θ) can be calculated in the FAST.Farm coordinate system as:

$$\sigma = \frac{N_z}{A} - \frac{M_x}{I_x} r\cos(\theta) + \frac{M_y}{I_y} r\cos(\theta) \tag{2}$$

where N_z is the axial force, M_y and M_z are the bending moments, I_x and I_y are the second moments of area, and A is the cross-sectional area. In the present work, we do not examine fatigue damage due to shear stresses as they were found to be significantly smaller than damage from axial stresses. By considering zero bending moments, Equation 2 can also be used to calculate the axial stresses at the midpoint of the cross-section closest to the fairlead of the mooring lines.

Using the time history of the stress, the number of load cycles at different stress levels is computed using a rainflow cycle counter. Rainflow cycle counting is implemented using WAFO [32] and the 1-h fatigue damage was found using Palmgren-Miners rule with a modification to allow for two-slope S-N curves. Additionally, a low-pass filter with a cutoff frequency of 3 Hz was applied to reduce the impact of high-frequency oscillations from noise in the fairlead tension time-series output on the mooring line fatigue damage calculations.

Representative S-N curves were selected for the tower using DNV-RP-C203 [33] and for the fairlead of the mooring lines using DNVGL-OS-E301 [34], as described in Table 6. S-N curves for girth welds are used for the tower.

Table 6: S-N curves used in fatigue damage calculations [33, 34].

	m_1	$\log_{10}(K_1)$	Maximum N_1	m_2	$\log_{10}(K_2)$	S-N Curve
Tower	3.0	12.164	1×10^{-7}	5.0	15.606	2-1, D
Mooring lines	3.0	10.778	-	-	-	Studless Chain

3. Results and Discussion

3.1. Flow Field

The ambient wind fields generated using Kaimal - Coh u, v, w and Mann both result in considerable lateral meandering of FWT1's wake center at $8D$ as seen in the left subplot of Figure 3. In the middle subplot of the same figure, we can see from the averaged probability density functions (PDFs) that the Kaimal - Coh u, v, w simulations have greater variance in the lateral wake center position than the Mann simulations ($0.37D^2$ compared to $0.15D^2$). Inflow generated using the Kaimal - Coh u method results in no significant lateral meandering. However, it is important to also mention that because of the relatively high TI, the wake deficit of FWT1 may be weak by the time it reaches FWT2's rotor plane. While the three approaches result in very different levels of lateral meandering, the magnitude of vertical meandering (not shown) was not found to be sensitive to the three methods.

For the Kaimal - Coh u, v, w and Mann simulations, the movement of FWT1's lateral wake center is on the order of 0.1-0.2 Hz (50-100 s). The spectrum of FWT1's lateral wake center position at $8D$ is shown in Figure 3. The Kaimal - Coh u, v, w inflow results in the most low-frequency response, and includes components at somewhat higher frequencies than the Mann inflow.

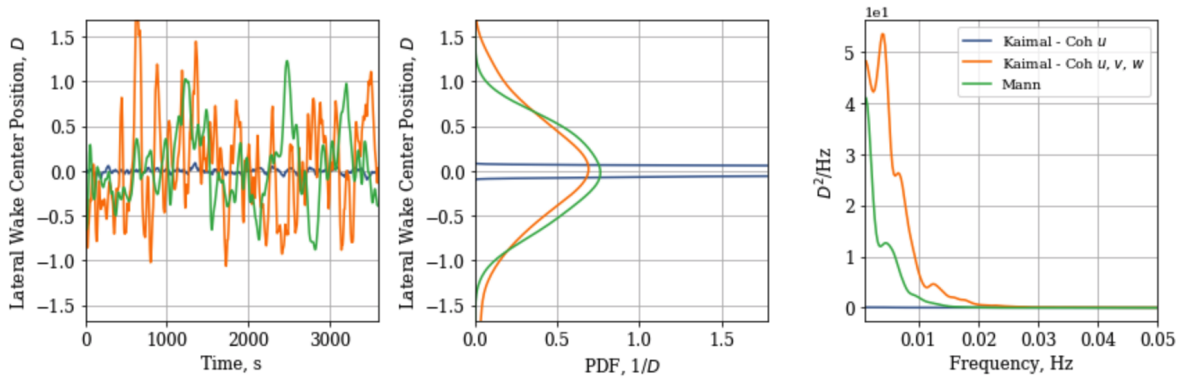

Figure 3: Time series for a single simulation (left), PDF averaged over six simulations (middle), and averaged spectra (right) of FWT1's lateral wake center position at $8D$

An instantaneous flow visualization of U in the XY-plane for a single realization using the three methods for generating inflow are shown in Figure 4. The ambient wind flow looks similar for Kaimal - Coh u and Kaimal - Coh u, v, w because only the v- and w-velocity components of the wind differ considerably. Even though the lateral and vertical velocity components are small in relation to U, they substantially affect the meandering pattern of the wake. This effect is understandable given that wake meandering is driven by large-scale turbulence.

While the Mann inflow has similar U and TI, it contains longer coherent shapes in the XY plane. As explained by Eliassen and Bachynski [20], these coherent structures in the horizontal plane dominate the Mann turbulence model, whereas, the Kaimal turbulence model distributes coherent shapes evenly in horizontal, vertical, and diagonal directions. This has a significant effect on the turbine response, which is discussed in the following sections.

Figure 5 shows the hub-height wind speed and turbulence intensity and Table 7 lists the mean 3P frequency for FWT1 and FWT2. The decrease in U and rotor speed from FWT1 to FWT2 is strongly correlated with the variance in the FWT1's lateral wake center position at $8D$. As FWT2 constantly operates in a fully waked state in the Kaimal - Coh u simulations, it experiences the largest decrease in hub-height wind speed. FWT2 experiences the smallest decrease in U and greatest increase in TI for the Kaimal - Coh u, v, w inflow, that is, the inflow with the most meandering.

Table 7: Mean 3P frequencies of each FWT.

	FWT1	FWT2
Kaimal - Coh u	0.387 Hz	0.336 Hz
Kaimal - Coh u, v, w	0.387 Hz	0.345 Hz
Mann	0.386 Hz	0.358 Hz

3.2. Platform Motions

The standard deviations of the rigid body surge (η_1), pitch (η_5), and yaw (η_6) motions are shown in Figure 6. For the Kaimal - Coh u simulations, FWT1 and FWT2 had similar standard deviations in surge and pitch and a 5.5 % decrease for FWT2 in yaw. When using the Kaimal - Coh u, v, w and Mann inflows, which result in significant wake meandering, a greater standard deviation in surge, pitch and (especially) yaw is seen in FWT2 compared to FWT1. The standard deviation in surge and pitch increases for FWT2 compared to FWT1 between 5 % and 8 % for

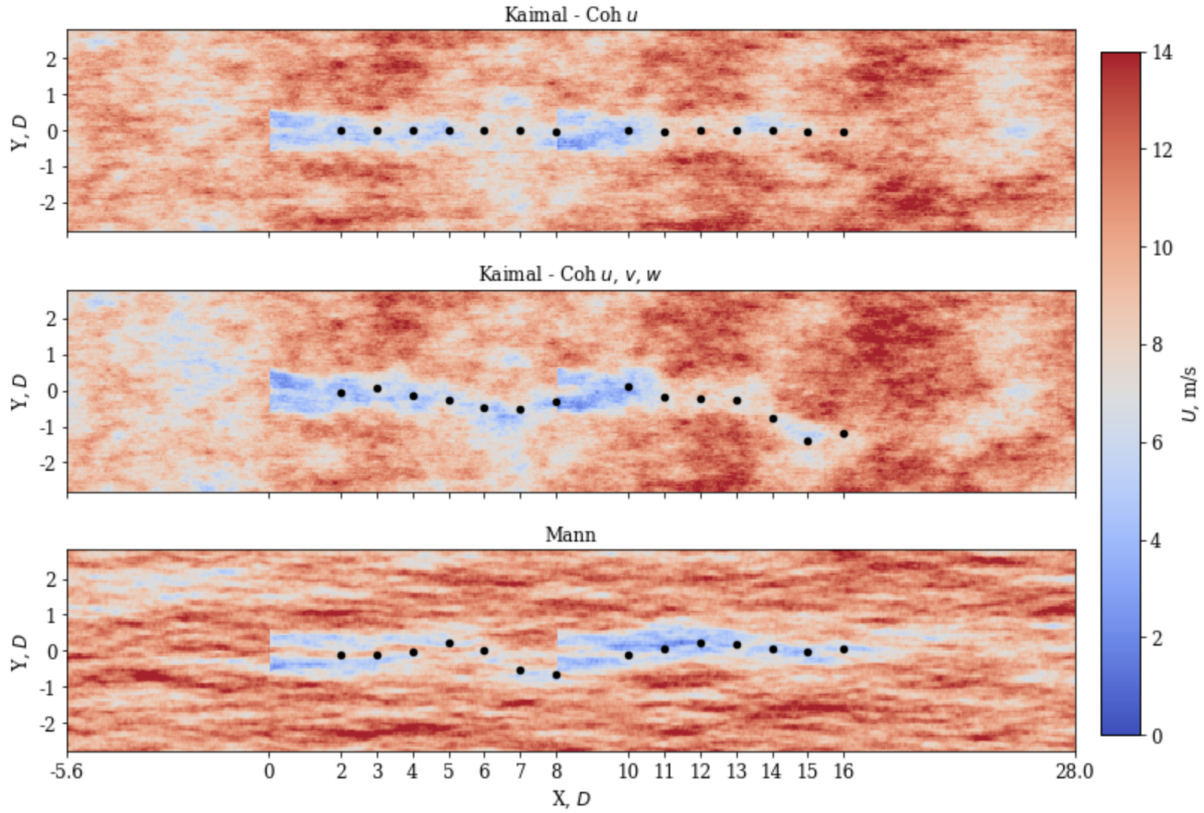

Figure 4: Instantaneous flow visualization of the wind speed at hub-height in the XY-plane. The wake centers at different distances downstream are output by FAST.Farm and represented by black dots.

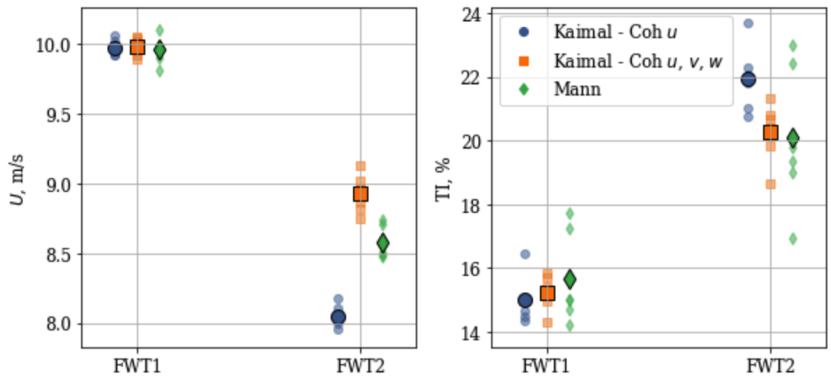

Figure 5: Hub-height wind speed (left) and turbulence intensity (right) for FWT1 and FWT2 for each inflow method. The average value of each of the six realizations is larger and outlined in black.

the Kaimal - Coh u, v, w and Mann inflows, while the standard deviation in yaw increases by 28.0 % for Kaimal - Coh u, v, w and 11.3 % for Mann.

Additionally, the low-frequency movement in the meandering wake results in increased low-frequency response in the platform motions. This increase in response is most apparent when

looking at the spectrum of the yaw motion, but is also visible in the surge and pitch motion spectra (Figure 7). From Figure 7, both the low-frequency quasi-static response and the response at the yaw natural frequency are larger for FWT2 compared to FWT1, for the Mann simulations and especially for the Kaimal - Coh u, v, w simulations. However, the yaw motions of FWT1 and FWT2 are almost equivalent for the Kaimal - Coh u simulations.

For FWT1, the surge and pitch standard deviations are lower while the yaw standard deviation is greater for the Mann turbulence model compared to the simulations utilizing the Kaimal turbulence model. These trends are consistent with previous research [20, 24]. Furthermore, Eliassen and Bachynski suggest that the decreased response in yaw for the Kaimal turbulence model can be related to the largest coherent structures: these tend to come in pairs with opposing diagonal symmetry passing through the center of the domain, unlike the non-centered structures with symmetry about horizontal or vertical planes that are found in Mann turbulence model [24]. The Kaimal turbulence model gives a more evenly distributed force over the rotor and therefore also larger response in surge compared to the Mann turbulence model.

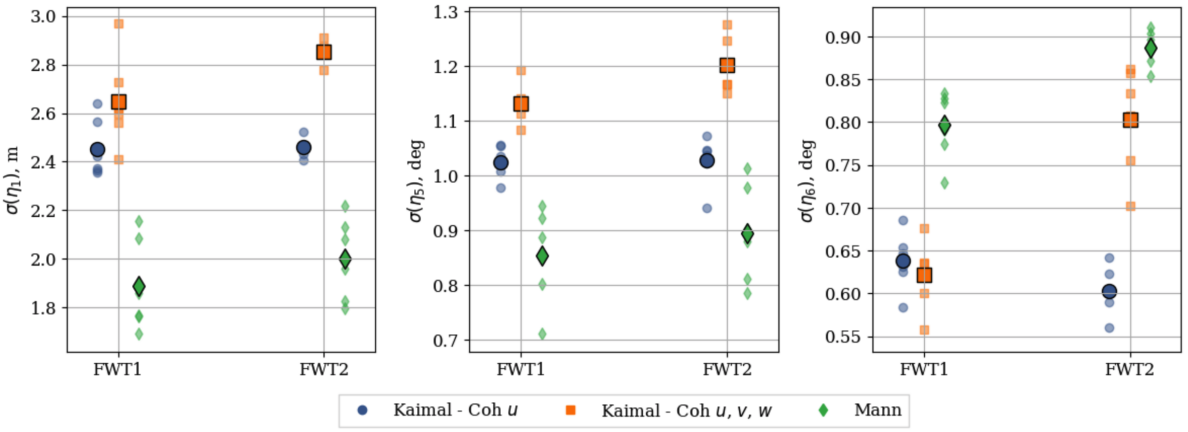

Figure 6: Surge (left), pitch (middle), and yaw (right) standard deviations $\sigma(\eta)$. The average value of each of the six realizations is larger and outlined in black.

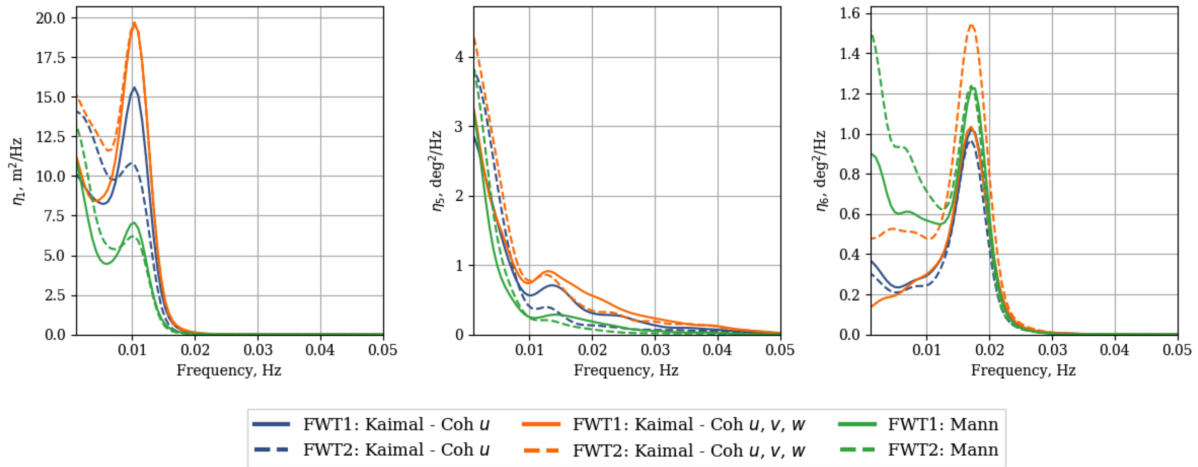

Figure 7: Surge (left), pitch (middle), and yaw (right) spectra.

3.3. Fatigue Analysis

To investigate the effect of wakes on the structural response of the downstream turbine, we examine the 1-h fatigue damage at the base of the tower, top of the tower, and at the fairlead of each of the three mooring lines.

In the tower base and tower top, the fatigue damage D_{RFC} due to axial stress σ is calculated at 24 points around the cross-section. The greatest damage in FWT1 and FWT2 for all three methods occurred at the downstream point of the cross-section along the fore-aft axis except for FWT2 in Mann simulations where it occurred at the upstream point. The fatigue damage in the tower base and tower top at the downstream point is shown in Figure 8. The damage in the tower base is only greater (2.0 % increase) in FWT2 to that of FWT1 for the Kaimal - Coh u, v, w simulations.

The spectra of axial stress σ in the tower base and top are shown in Figure 9, and are separated into low-, wave-, and tower- ranges for clarity (note the varying scales for the vertical axes). The coupled pitch and tower bending frequencies (0.39 and 0.44 Hz) are excited by 3P at the tower base. Even though there is relatively low energy in the 3P frequency range compared to lower frequencies, the responses in the 3P range significantly influence the short-term fatigue damage due to their large number of cycles. Additionally, this problem is exacerbated for the Mann simulations as the Mann turbulence model results in greater response at 3P (consistent with previous studies [20, 24]), leading to the greatest damage. Similar to observations for the platform motions, the spectra of axial stress σ in the tower base and tower top are greater in FWT2 compared to FWT1 at lower-frequencies for Kaimal - Coh u, v, w and Mann due to wake meandering.

The mean fatigue damage at the tower top is smaller than that at the base. However, the fatigue damage at the tower top is less sensitive to tower bending, which makes it useful in isolating wake-induced fatigue. As expected, the fatigue damage is greater in FWT2 for all three inflows, due to increased TI (see Figure 5). The fatigue damage increased by 15.6 % for Kaimal - Coh u, 30.4 % for Kaimal - Coh u, v, w and 2.0 % for Mann. Again, we see that the Mann turbulence model results in much greater 3P response compared to inflow generated using the Kaimal turbulence model, leading to significantly greater fatigue damage. Also demonstrated in Figure 9, more energy is present at lower-frequencies for FWT2 compared to FWT1 for inflows that induce meandering.

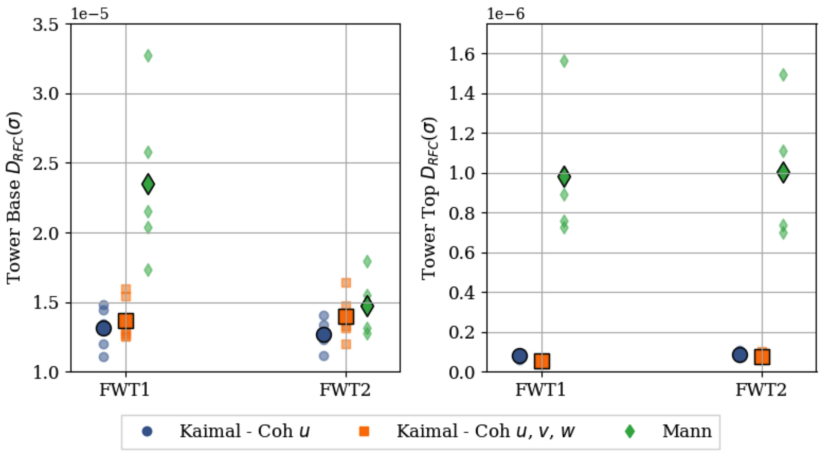

Figure 8: Fatigue damage at the tower base (left) and tower top (right). The average value of each of the six realizations is larger and outlined in black.

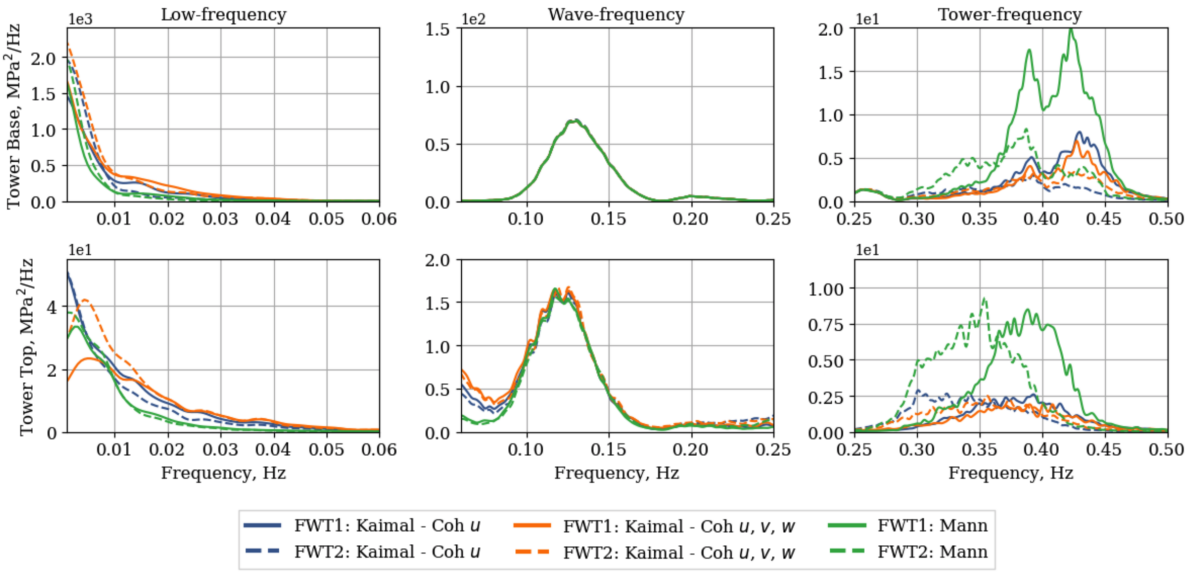

Figure 9: Tower base (top) and tower top (bottom) axial stress σ spectra.

The mean 1-h fatigue damage for each mooring line is shown in Figure 10. Regardless of turbulence model and inflow type, the highest damage occurred in the upstream turbine and in mooring line 1.

The mooring line spectra are shown in Figure 11 and are similarly separated by low-, wave-, and tower-frequency ranges for clarity. The surge frequency is dominant among the lower frequencies. The downstream turbine for the second and third methods has a greater response at low frequencies compared to the upstream turbine due to wake meandering. There are important responses at the coupled pitch and tower bending frequencies and 3P, which are drivers for the fatigue damage in the mooring lines. Additionally, there is a slight mean roll offset due to the rotor torque moment, which is why mooring lines 1 and 2 have different responses. The mean roll offset increases the stiffness in mooring line 1 resulting in greater high-frequency excitation. Similar to the stresses in the tower base and tower top, the 3P response is greater for the Mann turbulence model which is why the mooring lines experience greater fatigue damage than that from simulations using the Mann turbulence model - despite the large surge motions with the Kaimal model.

4. Conclusions and Future Work

The objective of this work is to investigate how the wake interaction between two CSC 10 MW FWTs affects global responses. Three different methods were used to generate synthetic turbulent turbulent inflow, as it was found that the spatial coherence in the lateral direction has a significant impact on the turbine's wake meandering pattern. The first method, Kaimal - Coh u, only has spatial coherence in the longitudinal velocity component and results in a uniform, axial wake deficit with negligible meandering. The second method, Kaimal - Coh u, v, w, has spatial coherence in the longitudinal, lateral, and vertical velocity components which induces meandering of the lateral wake center with a standard deviation of $0.6D$ at the downstream turbine's rotor plane ($8D$). The third method, Mann, where spatial coherence is inherent in the model, results in slightly less meandering, a standard deviation of $0.4D$, than the second method.

The Kaimal - Coh u, v, w and Mann methods for generating inflow result in meandering of

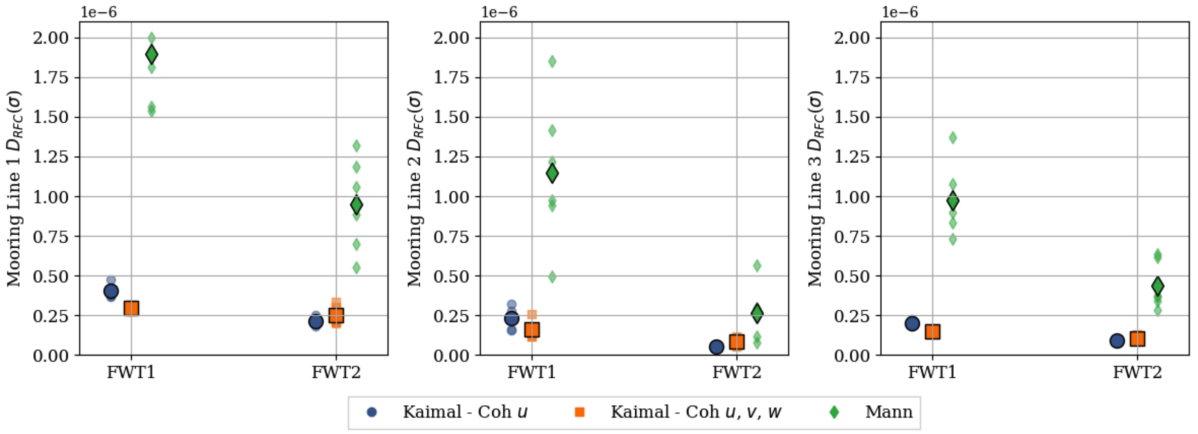

Figure 10: Fatigue damage at the fairlead in mooring line 1 (left), mooring line 2 (middle), and mooring line 3 (right). The average value of each of the six realizations is larger and outlined in black.

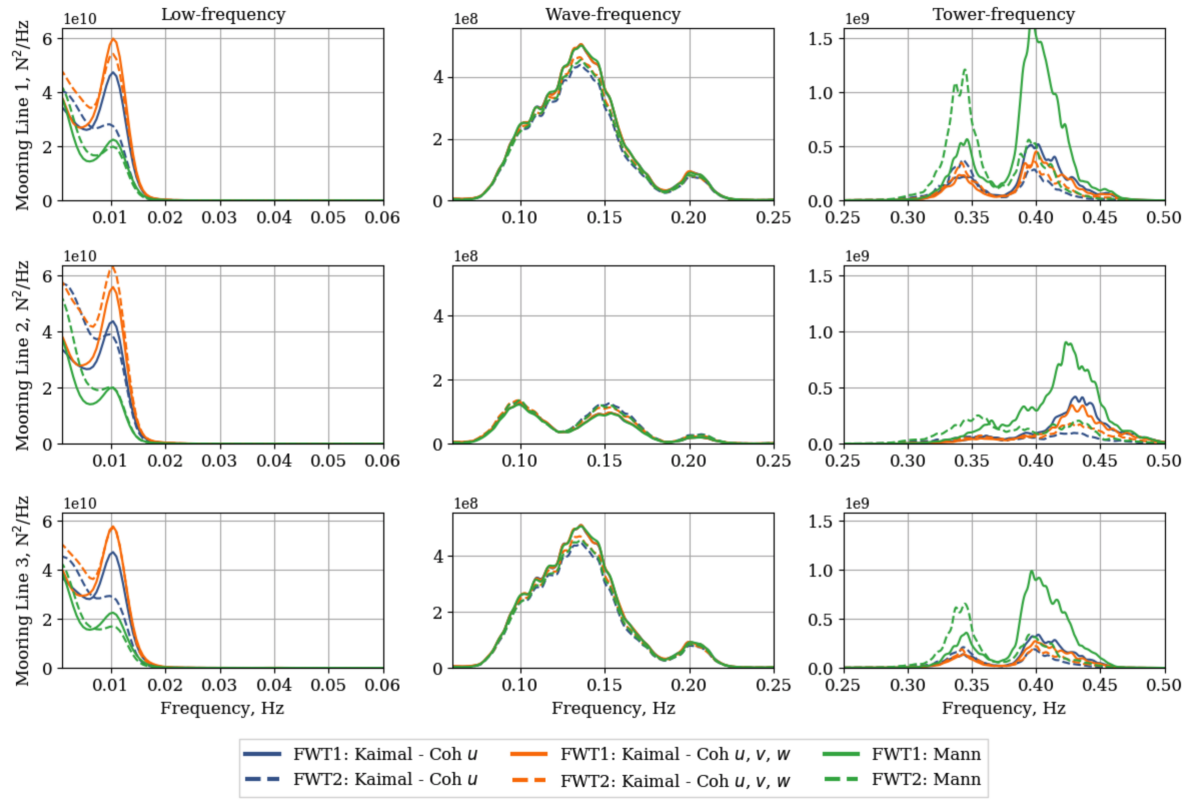

Figure 11: Mooring line 1 (top), 2 (middle), 3 (bottom) tension spectra.

the wake at frequencies on the order of 0.01-0.02 Hz (50-100 s), with slightly higher frequencies present in Kaimal - Coh u, v, w. As expected, the large-scale, low-frequency movement of the upstream turbine's wake has a significant impact on the downstream turbine's responses. The standard deviation in surge and pitch increases for FWT2 compared to FWT1 between 5 % and 8 % for Kaimal - Coh u, v, w and Mann inflows, while the standard deviation in yaw

increases by 28.0 % for Kaimal - Coh u, v, w and 11.3 % for Mann. Low-frequency motion in surge, pitch, and yaw increases for the downstream turbine, FWT2, compared to the upstream turbine, FWT1. While low-frequency responses increase due to wake meandering, this did not always result in greater fatigue damage. Due to the placement of the tower bending natural frequency, the CSC 10 MW is particularly sensitive to 3P excitation. In the tower base and mooring lines, the fatigue damage was always greater for FWT1 than for FWT2 when using the Kaimal - Coh u and Mann inflows. Consistent with other studies, it was found that the Mann turbulence model results in greater response in the blade passing frequency range, which had a significant effect on fatigue. With reduced 3P excitation from the Kaimal turbulence model, the fatigue damage in the tower base of FWT2 increases by 2.0 % compared to FWT1 due to wake meandering. At the tower top, where responses are less sensitive to tower bending, the fatigue damage increases between 2 % and 30 % for all three inflows.

This work suggests a need for further study into the mooring and tower base fatigue damage for different FWT concepts with more representative structural design of the tower, or with modifications made to the wind turbine control system. Additionally, it would be interesting to compare results with other FWT concepts that are particularly sensitive to yaw motions, such as a spar.

Acknowledgments

The corresponding author acknowledges support from the U.S.-Norway Fulbright Foundation. Thank you to Pietro Bortolotti of NREL for providing the AeroDyn v15 input file of the rotor. Discussions with Lene Eliassen and Marit Kvittem of SINTEF Ocean and Jason Jonkman of NREL are also appreciated.

References

[1] Statoil 2014 Hywind Scotland Pilot Park URL http://www.statoil.com/en/TechnologyInnovation/NewEnergy/RenewablePowerProduction/Offshore/HywindScotland
[2] Vermeulen P E J 1980 *3rd International Symposium on Wind Energy Systems* ed Downey W T pp 431–450
[3] Ainslie J 1988 *Journal of Wind Engineering and Industrial Aerodynamics* **27** 213–224 ISSN 01676105 URL http://linkinghub.elsevier.com/retrieve/pii/0167610588900372
[4] Larsen T and Hanson T 2007 *Journal of Physics: Conference Series, The Second Conference on The Science of Making Torque from Wind* **75**
[5] Madsen H A, Larsen G C, Larsen T J, Troldborg N and Mikkelsen R 2010 *Journal of Solar Energy Engineering* **132** 041014 ISSN 01996231 URL http://SolarEnergyEngineering.asmedigitalcollection.asme.org/article.aspx?articleid=1458224
[6] Churchfield M, Lee S, Moriarty P, Martinez L, Leonardi S, Vijayakumar G and Brasseur J 2012 *50th AIAA Aerospace Sciences Meeting including the New Horizons Forum and Aerospace Exposition* (Nashville, Tennessee: American Institute of Aeronautics and Astronautics) ISBN 978-1-60086-936-5 URL http://arc.aiaa.org/doi/10.2514/6.2012-537
[7] Lee S, Churchfield M, Moriarty P, Jonkman J and Michalakes J 2012 *50th AIAA Aerospace Sciences Meeting including the New Horizons Forum and Aerospace Exposition* (Nashville, Tennessee: American Institute of Aeronautics and Astronautics) ISBN 978-1-60086-936-5 URL http://arc.aiaa.org/doi/10.2514/6.2012-540
[8] Larsen T J, Larsen G, Madsen H A and Petersen S M 2015 *EWEA Annual Conference and Exhibition* (Paris, France)
[9] Larsen T J, Larsen G C, Aagaard Madsen H, Thomsen K and Markkilde Peterson S 2015 Comparison of measured and simulated loads for the Siemens SWT 2.3 operating in waked conditions at the Lillgrund Wind Farm using HAWC2 and the dynamic wake meander model
[10] Jonkman J M, Annoni J, Hayman G, Jonkman B and Purkayastha A 2017 *35th Wind Energy Symposium* (Grapevine, Texas: American Institute of Aeronautics and Astronautics) ISBN 978-1-62410-456-5 URL http://arc.aiaa.org/doi/10.2514/6.2017-0454
[11] Jason Jonkman M B 2005 FAST Users Guide Technical Report NREL/EL-500-38230 National Renewable Energy Laboratory Golden, CO

[12] Jonkman B 2014 TurbSim Users Guide v2.00.00 Tech. Rep. NREL/TP-xxxx-xxxxx National Renewable Energy Laboratory Golden, CO
[13] Mann J 1998 *Probabilistic Engineering Mechanics* **13** 269–282
[14] Wang Q 2014 *Design and dynamic analysis of a steel pontoon-type semi-submersible floater supporting the DTU 10MW reference turbine* Master's thesis NTNU/TU Delft
[15] Luan C, Gao Z and Moan T 2016 *35th International Conference on Ocean, Offshore and Arctic Engineering* OMAE2016-54848 (Busan, South Korea)
[16] Bak C, Zahle F, Bitsche R, Kim T, Yde A, Henriksen L C, Natarajan A and Hansen M H 2013 Description of the DTU 10 MW Reference Wind Turbine Tech. Rep. DTU Wind Energy Report-I-0092 DTU Wind Energy
[17] Bottasso C L, Bortolotti P, Croce A and Gualdoni F 2016 *Multibody System Dynamics* **38** 317–344 ISSN 1384-5640, 1573-272X URL http://link.springer.com/10.1007/s11044-015-9488-1
[18] Sartori L, Bortolotti P, Croce A and Bottasso C L 2016 *Journal of Physics: Conference Series* **753** 062006 ISSN 1742-6588, 1742-6596 URL http://stacks.iop.org/1742-6596/753/i=6/a=062006?key=crossref.46db52bc37956c07d4541dcabf45d4ec
[19] Pegalajar-Jurado A, Madsen F J, Borg M and Bredmose H 2018 State-of-the-art models for the two LIFES50+ 10MW floater concepts Tech. Rep. D4.5 LIFES50+ Deliverable, project 640741
[20] Eliassen L and Bachynski E 2017 (*ASME 2017 36th International Conference on Ocean, Offshore and Arctic Engineering* no OMAE2017-61179) (Trondheim, Norway)
[21] Hall M 2015 MoorDyn User's Guide Tech. rep. Department of Mechanical Engineering, University of Maine Orono, ME
[22] Doubrawa P, Annoni J R and Jonkman J M 2018 *2018 Wind Energy Symposium* (Kissimmee, Florida: American Institute of Aeronautics and Astronautics) ISBN 978-1-62410-522-7 URL https://arc.aiaa.org/doi/10.2514/6.2018-0512
[23] International Electrotechnical Commission (IEC) 2005 Wind turbines: Part 1: Design requirements Tech. Rep. IEC61400-1:2005
[24] Bachynski E E and Eliassen L 2018 *Wind Energy* **22** 219–238 URL https://onlinelibrary.wiley.com/doi/abs/10.1002/we.2280
[25] Godvik M 2016 Science meets Industry (Stavanger) URL http://www.norcowe.no/doc//konferanser/2016/SMI%20Stavanger%20presentasjoner/Godvik%20Statoil%20Influence%20of%20the%20wind%20coherence%20on%20the%20response%20of%20a%20floating%20wind%20turbine.pdf
[26] DTU Wind Energy 2014 Pre-processing tools - HAWC2 URL http://www.hawc2.dk/download/pre-processing-tools
[27] Shaler K, Jonkman J, Doubrawa P and Hamilton N *36th Wind Energy Symposium* (San Diego, California: American Institute of Aeronautics and Astronautics)
[28] Mann J 1994 *Journal of fluid mechanics* **273** 141–168
[29] Li L, Gao Z and Moan T 2013 (*32nd International Conference on Ocean, Offshore, and Arctic Engineering* no OMAE2013-10156)
[30] International Electrotechnical Commission (IEC) 2009 Wind turbines: Part 3: Design requirements for offshore wind turbines Tech. Rep. IEC61400-3
[31] Kvittem M I and Moan T 2015 *Marine Structures* **40** 38–59
[32] Brodtkorb P, Johannesson P, Lindgren G, Rychlik I, Rydén J and Sjö E 2000 (*Proc. 10th Int. Offshore and Polar Eng. Conf., ISOPE, Seattle, USA* vol 3) (International Society of Offshore and Polar Engineers) pp 343–350
[33] Det Norske Veritas 2010 Fatigue design of offshore steel structures Tech. Rep. DNV-RP-C203
[34] Det Norske Veritas 2010 Position mooring Tech. Rep. DNV-OS-E301